Aeroacoustics Conferences
20-23 May 2019, Delft, The Netherlands
25th AIAA/CEAS Aeroacoustics Conference

10.2514/6.2019-2756

Shooting Method for Linear Inviscid Bi-Global Stability Analysis of Non-Axisymmetric Jets

Nikhil Sohoni * and Aniruddha Sinha †

Aerospace Engineering, Indian Institute of Technology Bombay, Powai, Mumbai 400076, INDIA

The shooting method is commonly used to solve the linear parallel-flow stability problem for axisymmetric jets, as well as planar flows, that have one inhomogeneous direction. The present extension to two inhomogeneous directions (i.e., bi-global stability problem) is motivated by inviscid non-axisymmetric jets. The azimuthal direction is Fourier transformed to obtain a set of coupled one-dimensional shooting problems that are solved by two-way integration from either radial boundary. The overall problem is formulated as one of iterative root-finding to match the solutions from the two integrations. The approach is validated against results from the well-established direct matrix method that discretizes the domain to obtain a matrix eigenvalue problem. We demonstrate very good agreement in two jet problems – an offset dual-stream jet, and a jet exiting from a nozzle with chevrons.

I. Introduction

Although axisymmetric (round) jets constitute a benchmark flow for their azimuthal homogeneity, practical prerogatives dictate the prevalence of non-axisymmetric jets in engines. The azimuthal inhomogeneity of such jets may be preferred, either for promoting mixing to reduce noise radiation, or for redirecting the noise away from the bottom sector of the jet. The former is exemplified by jets exiting from nozzles with chevrons[1], and by jets from round nozzles having additional micro-jets impinging at their lip[2]. An instance of the latter is a dual-stream jet where the two streams are not coaxial, but instead have an offset between them such that the secondary potential core is thickened in the bottom sector[3].

The linear Kelvin-Helmholtz (K-H) instability mode of the time-averaged flow field of turbulent jets is a useful model of their noise sources[4]. A quasi-parallel flow assumption is often valid as the jet displays a slow streamwise spread. In case of axisymmetric jets, the consequent spatial stability analysis reduces to an eigenvalue problem involving an ordinary differential equation (ODE) in the radial coordinate, separately for every pair of frequency and azimuthal Fourier mode of fluctuation. However, for non-axisymmetric jets the problem becomes one of bi-global stability involving partial differentials in both the radial and azimuthal coordinates. This means that, in the Fourier azimuthal domain, although the linear stability equations still involve ordinary derivatives in the radial coordinates only, the various azimuthal Fourier modes of the eigenfunction are coupled for a particular frequency of perturbation. The latter problem has been solved using the direct matrix method[5–8]. In this approach, the system of coupled ODEs is converted into a matrix eigenvalue problem by suitable discretization of the radial domain.

In this paper, we adopt the alternative approach of shooting. In this method, the differential eigenvalue problem with boundary conditions is posed as an initial-value problem. The eigenvalue is guessed to start with. In the one-way shooting method, the eigenfunction is integrated starting from one boundary and proceeding towards the other. The satisfaction of the boundary condition thereat is obtained in an iterative manner by improving the guess of the parameters of the problem that include the eigenvalue. In the two-way shooting approach, the integration is started separately from both boundaries, and approach each other at an intermediate point. The matching of the two eigenfunction solutions at this point is again achieved in an iterative manner.

The shooting method is preferred over the matrix method whenever (a) a single eigensolution is desired, and (b) a good initial guess is available for it. The bi-global stability problem will be seen to have multiple

*Graduate student
†Associate Professor; AIAA Member; Corresponding author: as@aero.iitb.ac.in

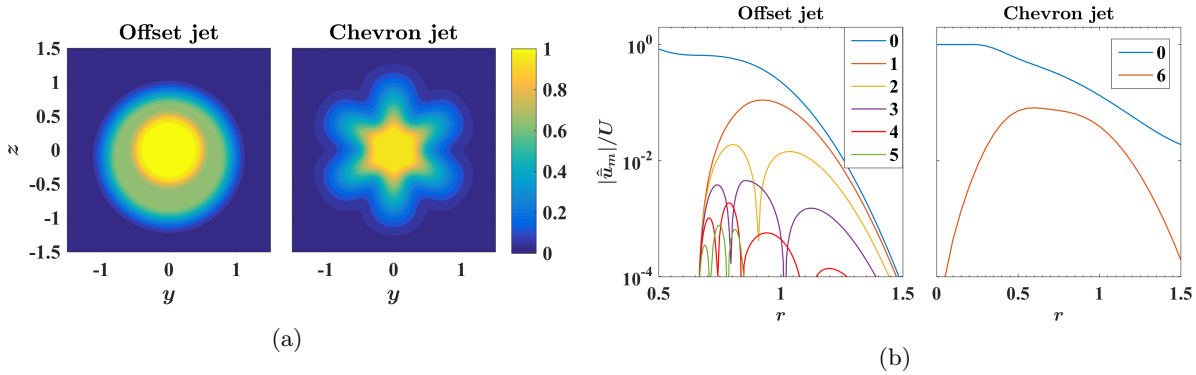

Figure 1: (a) Mean axial velocity fields of the two jets analyzed – dual-stream jet with offset of $0.1D_p$ at $x = 2D_p$, and jet from chevron nozzle at $x = 3D$. The colorscale represents $\overline{u}$ normalized by the respective (primary) jet exit velocities. (b) Non-trivial azimuthal Fourier modes of these mean flow fields.

unstable K-H modes as solutions, and shooting may be used conveniently for 'tracking' these modes individually as some relevant condition (like axial station, Strouhal number, offset between the two jet streams, etc.) is varied.

The shooting method has been used in non-axisymmetric jet stability analysis earlier by Gudmundsson [6]; here we report on some improvements to the procedure. Specifically,

- We use a two-way shooting approach whereas the reference work employed a one-way method; this bestows greater numerical stability to the computations.
- For faster and more reliable convergence, we calculate the necessary Jacobian of the cost function (see more later) analytically instead of the numerical computation employed in the reference.
- We explicitly account for the mirror symmetry of the problem, thereby reducing the problem size.

We provide validation of our shooting algorithm against the matrix method solution for an offset jet and a jet exiting from a nozzle with chevrons.

II. Jets Analyzed for Validation

To motivate the development of the stability theory subsequently, we start by describing the kinds of non-axisymmetric jets that will serve as test cases for validation.

In a companion paper [9], we have described the mean axial velocity function of a dual-stream jet that can be assigned an arbitrary offset. There we have used the matrix method to analyze such jets with various offsets at a range of axial stations. Here, one of the validation studies uses the same jet. In particular, the ratio of the secondary to primary nozzle exit diameters (D_s/D_p) is 1.7, the exit Mach numbers of the primary and secondary streams are respectively 1.5 and 0.9, the entire jet is at ambient temperature such that there are no mean density variations, and the offset between the two streams is $0.1D_p$. The axial station at which the analysis is performed is $x = 2D_p$; fig. 1a shows the mean axial velocity thereat. All length dimensions are normalized by D_p, and the temporal frequency ω analyzed is reported in terms of the Strouhal number $St := \omega D_p/(2\pi U_p)$, where U_p is the primary jet exit velocity.

The second jet analyzed is the one exiting at Mach 0.9 from the SMC001 6-chevron nozzle designed and tested by Bridges and Brown [1]. The mean flow field originally measured with particle image velocimetry is smoothed by fitting functions described by Sinha et al. [7]. The stability analysis is performed on the mean axial velocity field at $x = 3D$ shown in fig. 1a (where D is the nominal nozzle exit diameter). The jet had a co-flow of Mach 0.01. The density field is again assumed to be uniform. In this case, length dimensions are normalized by D, and $St := \omega D/(2\pi U)$ with U as the jet exit velocity.

III. Inviscid Linear Bi-global Stability Theory for Non-axisymmetric Jets

We use cylindrical coordinates (x, r, θ) even though the formulation is for non-axisymmetric jets, as the reference case is invariably an axisymmetric jet. Let $\boldsymbol{q} := (u, v, w, p, \rho)^{\mathrm{T}}$ be the flow variable vector involving the axial, radial and azimuthal velocity components, and pressure and density, respectively. The usual Reynolds decomposition is performed on $\boldsymbol{q}$ to obtain the time-averaged mean $\overline{\boldsymbol{q}}$ and the residual fluctuations $\boldsymbol{q}'$. Assuming the mean flow to be locally parallel in x and stationary in time t, the linearity of the governing equations allow the following normal mode ansatz for $\boldsymbol{q}'$

$$\boldsymbol{q}'(x, r, \theta, t) = \tilde{\boldsymbol{q}}_\omega(r, \theta)\mathrm{e}^{\iota(\alpha x - \omega t)} + \text{c.c.} \tag{1}$$

In spatial stability analysis, $\tilde{\boldsymbol{q}}$ is the shape function corresponding to a specified real angular frequency ω and the complex wave number α is to be determined. The latter's real part α_r signifies the actual wave number (inversely proportional to the phase speed) and its imaginary part α_i corresponds to the decay rate (negative of growth rate).

An inviscid analysis is typically warranted since the K-H instability is essentially an inviscid phenomenon and the jets under study have high Reynolds number. Then, substituting the above ansatz in the linearized compressible Euler equation obtains the usual compressible Rayleigh equation for pressure fluctuations. For the non-axisymmetric jets under analysis here, it takes the following bi-global form [5]

$$\frac{1}{r}\frac{\partial}{\partial r}\left(r\frac{\partial \tilde{p}_\omega}{\partial r}\right) + \frac{1}{r^2}\frac{\partial^2 \tilde{p}_\omega}{\partial \theta^2} - \overline{f}\frac{\partial \tilde{p}_\omega}{\partial r} - \overline{g}\frac{1}{r^2}\frac{\partial \tilde{p}_\omega}{\partial \theta} - \overline{h}\tilde{p}_\omega = 0\ . \tag{2}$$

Here, the space-varying coefficients $\overline{f}$, $\overline{g}$ and $\overline{h}$ are functions of the mean flow field $\overline{\boldsymbol{q}}$ apart from α and ω:

$$\overline{f} = \frac{2\alpha}{\alpha\overline{u} - \omega}\frac{\partial \overline{u}}{\partial r} + \frac{1}{\overline{\rho}}\frac{\partial \overline{\rho}}{\partial r}, \qquad \overline{g} = \frac{2\alpha}{\alpha\overline{u} - \omega}\frac{\partial \overline{u}}{\partial \theta} + \frac{1}{\overline{\rho}}\frac{\partial \overline{\rho}}{\partial \theta}, \qquad \overline{h} = \alpha^2 - \overline{\rho}\left(\alpha\overline{u} - \omega\right)^2. \tag{3}$$

Instead of solving this problem in the physical (r, θ) domain, we solve it in the Fourier azimuthal and physical radial domain. This facilitates subsequent specialization to axisymmetric jets, wherein the Fourier azimuthal modes of the solution are decoupled. Irrespective of the specific problem, the mean flow $\overline{\boldsymbol{q}}$ and the pressure mode $\tilde{p}$ can be expanded in their respective azimuthal Fourier modes owing to periodicity in θ

$$\overline{\boldsymbol{q}}(\theta) = \sum_{n=-\infty}^{\infty} \hat{\overline{\boldsymbol{q}}}_n \mathrm{e}^{\iota n\theta}, \quad \hat{\overline{\boldsymbol{q}}}_n := \frac{1}{2\pi}\int_{-\pi}^{\pi} \overline{\boldsymbol{q}}(\theta)\mathrm{e}^{-\iota n\theta}\mathrm{d}\theta; \quad \tilde{p}_\omega(\theta) = \sum_{n=-\infty}^{\infty} \hat{p}_{\omega,n}\mathrm{e}^{\iota n\theta}, \quad \hat{p}_{\omega,n} := \frac{1}{2\pi}\int_{-\pi}^{\pi} \tilde{p}_\omega(\theta)\mathrm{e}^{-\iota n\theta}\mathrm{d}\theta,$$

where we have omitted the $r-$dependence for notational compactness. For reference, fig. 1b shows the non-trivial azimuthal Fourier modes of the mean axial velocity fields of the jets studied here. The mean flow functions $\overline{f}$, $\overline{g}$ and $\overline{h}$ are also transformed similarly. With this, the Rayleigh equation becomes

$$\frac{1}{r}\frac{\partial}{\partial r}\left(r\frac{\partial \hat{p}_{\omega,m}}{\partial r}\right) - \frac{m^2}{r^2}\hat{p}_{\omega,m} - \sum_{n=-\infty}^{\infty}\left\{\hat{\overline{f}}_n\frac{\partial}{\partial r} + \frac{\iota\left(m-n\right)}{r^2}\hat{\overline{g}}_n + \hat{\overline{h}}_n\right\}\hat{p}_{\omega,m-n} = 0, \qquad \forall m. \tag{4}$$

Thus, for any non-axisymmetric jet, the eigensolutions are coupled in their azimuthal Fourier modes.

In general, our analysis is applicable up to the end of the potential core; beyond that the velocity gradients are gradual enough so as to stabilize most perturbations. Thus the base flow can be assumed to be locally uniform at $r = 0$. In the radial far field, the assumption of local uniformity of the base flow is always valid. So, at both boundaries, eqn. (4) simplifies to the modified Bessel equation, yielding the boundary conditions

$$\hat{p}_{\omega,m}(r = r^c) \sim I_m\left(\sqrt{\alpha^2 - \overline{\rho}_0\left(\alpha\overline{u}_0 - \omega\right)^2}r^c\right), \quad \hat{p}_{\omega,m}(r = r^f) \sim K_m\left(\sqrt{\alpha^2 - \overline{\rho}_\infty\left(\alpha\overline{u}_\infty - \omega\right)^2}r^f\right). \tag{5}$$

Here I_m and K_m are respectively the modified Bessel functions of first and second kind for azimuthal mode m. Also, the boundary conditions are enforced at a small non-zero radius r^c (to avoid the centreline singularity), and at a very large radius r^f, respectively. Finally, $\overline{\rho}_0$ and $\overline{\rho}_\infty$ are respectively the mean density at the jet centreline and the ambient, and $\overline{u}_0$ and $\overline{u}_\infty$ are the corresponding mean axial velocities. Unless there is a co-flowing jet, $\overline{u}_\infty$ will vanish in a laboratory setting.

As demonstrated here, the equations are decoupled in ω. So, for notational convenience, we will omit ω in the subsequent development wherever it is obvious from the context.

A. Specialization to base flows with rotational symmetry

Chevron nozzles usually have the chevrons distributed uniformly around the circumference[1]. Similarly, nozzles with secondary micro-jets also typically have these devices deployed uniformly in azimuth[2]. Thus, the mean flow field in such jets exhibit an L–fold rotational symmetry, where L is the number of chevrons, micro-jets, etc. (see fig. 1a for an example). In such cases, the mean flow field presents a corresponding sparsity in the Fourier azimuthal domain[5]:

$$\overline{\boldsymbol{q}}(r,\theta) = \sum_{j=-\infty}^{\infty} \hat{\overline{\boldsymbol{q}}}_{Lj}(r)\mathrm{e}^{\iota Lj\theta}. \tag{6}$$

This sparsity pattern induces a similar sparsity in the coefficient functions $\hat{\overline{f}}$, $\hat{\overline{g}}$ and $\hat{\overline{h}}$. As a consequence, the Rayleigh equation (see eqn. (4)) becomes

$$\frac{1}{r}\frac{\partial}{\partial r}\left(r\frac{\partial \hat{p}_m}{\partial r}\right) - \frac{m^2}{r^2}\hat{p}_m - \sum_{j=-\infty}^{\infty}\left\{\hat{\overline{f}}_{Lj}\frac{\partial}{\partial r} + \frac{\iota(m-Lj)}{r^2}\hat{\overline{g}}_{Lj} + \hat{\overline{h}}_{Lj}\right\}\hat{p}_{m-Lj} = 0, \qquad \forall m. \tag{7}$$

Equation (7) indicates that the $\hat{p}_m$ modes of the eigenfunction have a sparse coupling in the Fourier azimuthal domain in this case. In particular, the azimuthal mode m is coupled with the set $\{m+Lj\}_{j=-\infty}^{\infty}$. To distinguish between the different (decoupled) eigensolutions, we define the azimuthal order M as the central azimuthal mode of the above coupled set. For example, in the azimuthal order $M=0$ eigensolution, the set of coupled azimuthal modes is $\{Lj\}_{j=-\infty}^{\infty}$; that in the azimuthal order $M=1$ eigensolution is $\{1+Lj\}_{j=-\infty}^{\infty}$, and so on. Evidently, only mode orders $M=0$ to $M=L-1$ are unique, and need to be solved for. More details of the properties of the eigensolutions in this case have been described by Sinha et al.[7].

As an aside, note that the above formulation reduces to the general non-axisymmetric jet case if we set $L=1$, whereby all azimuthal modes are seen to be (densely) coupled. In this case, the only unique azimuthal order to solve for is $M=0$.

Practical mean flow fields can be represented by a finite set of modes, say $\{\hat{\overline{\boldsymbol{q}}}_{Lj}\}_{j=-N}^{N}$ in eqn. (6). Owing to their nonlinearity, the corresponding mean flow functions $\hat{\overline{f}}$, $\hat{\overline{g}}$ and $\hat{\overline{h}}$, have higher azimuthal complexity, say $\breve{N} \geq N$. Analogously, the eigensolutions will also converge with a finite coupled set of azimuthal modes in eqn. (7), say $\{\hat{p}_{M+Lj}\}_{j=-S}^{S}$, with $S \geq \breve{N}$.

It will be noted that, if L is even, then the Nyquist azimuthal order $M = L/2$ may be desired. In this case, symmetry considerations dictate that the coupled set of pressure eigenmodes to solve for is actually $\{\hat{p}_{L(j+1/2)}\}_{j=-S}^{S-1}$. In the remainder, this Nyquist azimuthal order will not be considered, as it requires special notation. This omission may be readily rectified by the interested reader.

B. Specialization to base flows with mirror symmetry

Often, the nozzle geometry has a plane of symmetry, as in offset multi-stream jets or nozzles with symmetric chevrons, such that the resulting jet mean flow field also has a corresponding symmetry (see fig. 1 for two examples). In such cases, choosing the plane of symmetry as the $\theta=0$ reference, the mean axial velocity and density fields can be written as cosine series, with purely real azimuthal Fourier modes

$$\overline{q}(r,\theta) = \sum_{j=0}^{\infty}(2-\delta_{j,0})\hat{\overline{q}}_{Lj}(r)\cos Lj\theta, \quad \hat{\overline{q}}_{Lj}(r) := \frac{1}{\pi}\int_0^{\pi}\overline{q}(r,\theta)\cos Lj\theta \,\mathrm{d}\theta, \qquad \overline{q}\in\{\overline{u},\overline{\rho}\}. \tag{8}$$

Correspondingly, the azimuthal Fourier modes of the coefficient functions have the following symmetry properties:

$$\hat{\overline{f}}_{-m} = \hat{\overline{f}}_m, \qquad \hat{\overline{g}}_{-m} = -\hat{\overline{g}}_m, \qquad \hat{\overline{h}}_{-m} = \hat{\overline{h}}_m. \tag{9}$$

Consequently, as shown in Appendix A, the pressure eigenfunctions are also symmetric, i.e., $\hat{p}_{-m} = \hat{p}_m$. Thus, in flows with mirror symmetry, the Rayleigh equation of eqn. (7) becomes

$$\frac{1}{r}\frac{\partial}{\partial r}\left(r\frac{\partial \hat{p}_m}{\partial r}\right) - \frac{m^2}{r^2}\hat{p}_m - \left(\hat{\overline{f}}_0\frac{\partial}{\partial r} + \hat{\overline{h}}_0\right)\hat{p}_m - \sum_{j=1}^{N}\left(\hat{\overline{f}}_{Lj}\frac{\partial}{\partial r} + \hat{\overline{h}}_{Lj}\right)\left(\hat{p}_{|m-Lj|} + \hat{p}_{|m+Lj|}\right)$$

$$-\frac{\iota}{r^2}\sum_{j=1}^{N}\hat{\bar{g}}_{Lj}\left\{(m-Lj)\hat{p}_{|m-Lj|}-(m+Lj)\hat{p}_{|m+Lj|}\right\}=0,\qquad \forall m\geq 0. \tag{10}$$

Note that the coupled azimuthal Fourier modes in the azimuthal order eigensolutions $M=1$ and $M=L-1$ are the same. Thus, the azimuthal orders to solve for are $M=0$ to $M=L/2$ if L is even, and up to $M=(L-1)/2$ if L is odd.

This symmetry is particularly advantageous for the azimuthal order $M=0$ eigensolution. In this case one needs to solve for only about half the total number of coupled azimuthal modes of the eigenfunction, viz. $\{\hat{p}_{Lj}\}_{j=0}^{S}$. This not only halves the problem size, but also enforces the symmetries of the eigensolution exactly. Recall that $M=0$ is the only azimuthal order to solve for in flows without rotational symmetry (i.e., when $L=1$), making the computational gains particularly striking.

C. Direct matrix method

The direct matrix approach for this problem has been established over the past few years in a series of publications[7–9]. Hence, we will treat the results from this method as the 'truth', and validate the shooting approach proposed here with respect to them. We briefly outline the direct matrix procedure here; the details can be found in the above references.

The normal mode ansatz for the fluctuations described above is applied to the set of five linearized governing equations. The resulting eigenvalue problem (coupled in the azimuthal Fourier domain) is discretized using fourth-order central differences on a radial grid that is clustered close to the primary nozzle's lip-line. The pole condition of Mohseni and Colonius[10] is applied at the centreline singularity, and the characteristic boundary condition of Thompson[11] is implemented at the far-field boundary ($r=r^f$). This results in a generalized matrix eigenvalue problem that is solved using the ARPACK library[12] in a parallelized fashion. The implementation allows for the viscous effects to be retained or turned off; inviscid computations are made for the present comparison.

The main parameters for this algorithm are (a) the azimuthal modal complexity of the mean axial velocity N, (b) that of the eigenfunction solution S, (c) the radial location of the far-field boundary r^f, and (d) the number of points in the radial grid N_r. The first three parameters are shared with the shooting method too, but it will be obvious subsequently that they have subtle differences in their implications.

IV. Shooting Method for the Bi-global Stability Problem

The shooting method is commonly used for solving two-point boundary value problems arising in one-dimensional linear stability problems[13]. To the knowledge of the authors, the only reported application in bi-global stability problems is the work of Gudmundsson[6]. Here, we solve the bi-global Rayleigh equation (see eqn. (7)) for both serrated and offset jets. Note that we need to determine an eigenvalue α and the corresponding pressure eigenfunction $\{\hat{p}_{\omega,M+Lj}\}_{j=-S}^{S}$ for a particular choice of frequency ω and azimuthal order M. The shooting method is most useful when only a few eigensolutions are desired, and good guesses are available for the corresponding eigenvalues. This happens to be the case for jet instability problems, as most often the K-H mode is the only one of interest.

In this work, we employ a two-way shooting method, extending the one-way shooting approach described by Gudmundsson[6]. The idea of a shooting method is to convert a two-point boundary value problem into an iterative initial value problem. We start with a guess of the eigensolution (that will be clarified below) at both the radial boundaries, and shoot (i.e., integrate) them towards each other using eqn. (7). At a certain intermediate radial point r_i, say, the two eigensolutions are compared through a cost function that is designed to be zero in case of a match. The process is necessarily iterative as the initial guesses have to be repeatedly improved with the aim of zeroing the cost function till convergence is achieved.

The shooting starts with a guess of the eigenvalue α that is to be refined progressively, and the integration of the pressure eigenfunction is initiated from both boundaries, i.e. from $r=r^c$ and $r=r^f$ (see eqn. (5)). We will denote these two eigenfunction solutions with superscripts $(\cdot)^c$ and $(\cdot)^f$ to respectively refer to the 'centre' and 'far' solutions integrated outward from the centreline and inward from the far field. Equation (5) indicates that, given the guess of α, one knows the eigenfunction $\hat{p}_m$ as well as its first derivative at both r^c and r^f for all $2S+1$ azimuthal modes involved. However, this is misleading since the relative amplitudes of the various $\hat{p}_m$'s must also be known – together the pressure modes have to satisfy the governing eqn. (7)

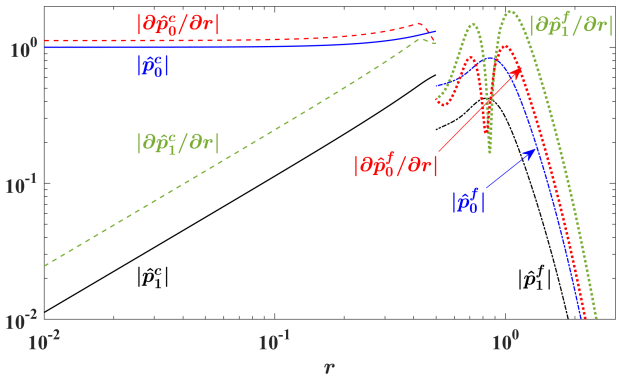

Figure 2: Pressure eigenfunctions in azimuthal modes $m = 0$ and 1 from the 'centre' and 'far' solutions, along with their radial derivatives, displaying the apparent mismatch at the intermediate point $r_i = 0.5$.

over the entire r–domain. Thus, we refine the definition of the initial (or boundary) conditions presented in eqn. (5), and write them compactly as

$$\hat{p}_m^\zeta(r^\zeta) = U_m^\zeta B_m(\lambda^\zeta r^\zeta), \qquad (\zeta, B) \in \{(c, I), (f, K)\}, \quad m \in \{M + Lj\}_{j=-S}^{S}. \tag{11}$$

Here, $\lambda^c := \sqrt{\alpha^2 - \overline{\rho}_0 \left(\alpha\overline{u}_0 - \omega\right)^2}$ and $\lambda^f := \sqrt{\alpha^2 - \overline{\rho}_\infty \left(\alpha\overline{u}_\infty - \omega\right)^2}$, and U_m^c and U_m^f are unknown complex scalar amplitudes. As the system is homogeneous, the overall amplitude of the eigenfunction is arbitrary so that one of the above complex scalars in each solution is a free variable; we set $U_M^c = U_M^f = 1$. Once these two values are fixed, all the remaining coupled azimuthal modes of the solution are fixed relative to each other. Thus, the vector of unknown parameters is

$$\boldsymbol{V} := \left(\alpha, U_{M-LS}^c, \cdots, U_{M-L}^c, U_{M+L}^c, \cdots, U_{M+LS}^c, U_{M-LS}^f, \cdots, U_{M-L}^f, U_{M+L}^f, \cdots, U_{M+LS}^f\right)^{\mathrm{T}}. \tag{12}$$

These parameters will be uniquely determined in the correct solution that we are iterating towards.

To initiate the integration of the second-order ODE that is eqn. (7), we not only calculate the pressure eigenmodes at either boundary from eqn. (11) using the guessed parameter vector, but also their respective radial derivatives:

$$\left.\frac{\partial\hat{p}_m^\zeta}{\partial r}\right|_{r=r^\zeta} = U_m^\zeta \lambda^\zeta B_m'\left(\lambda^\zeta r^\zeta\right), \qquad (\zeta, B) \in \{(c, I), (f, K)\}, \quad m \in \{M + Lj\}_{j=-S}^{S}. \tag{13}$$

Here, B' denotes the derivative of the Bessel function B with respect to its argument. The integration from the boundaries towards the intermediate point r_i employs the variable-step-size Runge-Kutta solver `ode45` in MATLAB®. For this, the second-order ODE is converted into a set of two coupled first-order ODEs.

Since U_M^c and U_M^f are chosen arbitrarily, the two solutions approaching from the two directions will not match at r_i in general (see fig. 2). However, in the correct eigensolution, the ratios of each $\hat{p}_m^c$ to the corresponding $\hat{p}_m^f$ must be same for all azimuthal modes m; similarly, the ratios of their respective radial derivatives should also match at r_i. We choose the value of $\hat{p}_M^c/\hat{p}_M^f$ at r_i as the common ratio to compare the ratios of all other modes and their radial derivatives. Thus, the set of cost functions to be zeroed are

$$\Lambda_m := \left(\hat{p}_m^c - \frac{\hat{p}_M^c}{\hat{p}_M^f}\hat{p}_m^f\right)\Bigg|_{r=r_i}, \qquad \Lambda_m' := \left(\frac{\partial\hat{p}_m^c}{\partial r} - \frac{\hat{p}_M^c}{\hat{p}_M^f}\frac{\partial\hat{p}_m^f}{\partial r}\right)\Bigg|_{r=r_i}, \qquad m \in \{M + Lj\}_{j=-S}^{S}. \tag{14}$$

Note that the cost function Λ_M is trivially zero. Thus, the non-trivial vector of cost functions is

$$\boldsymbol{\Gamma} := \left(\Lambda_{M-LS}, \cdots, \Lambda_{M-L}, \Lambda_{M+L}, \cdots, \Lambda_{M+LS}, \Lambda_{M-LS}', \cdots, \Lambda_{M-L}', \Lambda_M', \Lambda_{M+L}', \cdots, \Lambda_{M+LS}'\right)^{\mathrm{T}}. \tag{15}$$

It will be observed that, for a certain choice of the number of azimuthal modes of the eigensolution to retain in the calculation (i.e., S), the cost function vector above and the parameter vector $\boldsymbol{V}$ in eqn. (12) have the

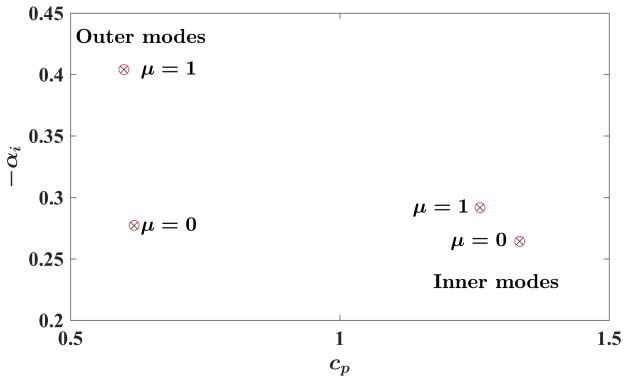

Figure 3: Offset jet: eigenvalues of the inner and outer modes for $\mu = 0$ and 1 for $St = 0.3$ at $x = 2$, obtained from the shooting method (black crosses) and direct matrix approach (red circles).

same number of elements, viz. $4S + 1$. In a mirror-symmetric problem for $M = 0$, the negative amplitude factors are omitted from $\boldsymbol{V}$, as are the cost functions for the negative azimuthal modes from $\boldsymbol{\Gamma}$. In this case the sizes of both $\boldsymbol{V}$ and $\boldsymbol{\Gamma}$ vectors are $2S + 1$.

The multi-dimensional Newton-Raphson method is used as the iterative algorithm to find the parameter vector $\boldsymbol{V}$ that zeroes the cost function vector $\boldsymbol{\Gamma}$. Specifically, for a trial $\boldsymbol{V}$, we evaluate $\boldsymbol{\Gamma}$ at the intermediate radial point r_i, as well as the Jacobian $\mathbb{J}$ of $\boldsymbol{\Gamma}$ with respect to $\boldsymbol{V}$ at this point. Then the Newton step for the parameter vector $\delta\boldsymbol{V}$ is given by the solution of the linear system of equations $\mathbb{J}\delta\boldsymbol{V} = -\boldsymbol{\Gamma}$. The problem is well-posed as $\boldsymbol{V}$ and $\boldsymbol{\Gamma}$ are vectors of the same size, so that the Jacobian $\mathbb{J}$ is a square matrix.

Unlike Gudmundsson[6] who evaluated the Jacobian numerically using multi-dimensional finite differences, we calculate it analytically as described in Appendix B. This requires additional quantities to be integrated from the boundaries along with the 'center' and 'far' pressure eigensolutions (see Appendix B). For a given choice of azimuthal complexity S, the resulting size of the vector to be integrated separately from each boundary becomes $4(S + 1)(2S + 1)$. In a mirror-symmetric problem for the $M = 0$ azimuthal order eigensolution, this size reduces to $2(S + 1)(S + 2)$.

V. Results

We present results from the study undertaken to validate the shooting method against the matrix method. The code is made general enough to handle both the offset multi-stream jet (having a mirror symmetry) and the jet exiting from the chevron nozzle (having rotational symmetry in addition to mirror symmetry), as described in § II.

A. Validation with offset dual-stream jet

The first validation case is the offset dual-stream jet, whose mean flow at $x = 2$ is considered (see fig. 1a). Stability calculations are performed for $St = 0.3$. The azimuthal modal complexity of the mean axial velocity field is set to $N = 3$ for both shooting and direct matrix approaches (see fig. 1b for reference). The inner and outer shear layers of such a dual-stream jet have respective inner and outer K-H instability modes associated with them[8,9,14]; we solve for both the modes here. As explained in § III, each eigensolution has many coupled azimuthal Fourier modes. However, typically one azimuthal mode can be found to dominate a particular eigensolution. We label the eigensolution dominated by the axisymmetric mode as $\mu = 0$, the one dominated by the first helical mode as $\mu = 1$, and so on; see Sohoni and Sinha[8] and Singh et al.[9] for more details. In this study, we solve for the $\mu = 0$ and 1 eigensolutions of both the inner and outer modes.

Before discussing the validation results, we present the eigensolutions for this problem (computed from the shooting method). Figure 3 shows the eigenspectrum, in terms of the growth rate $-\alpha_i$ vs. the phase speed $c_p := \omega/\alpha_r$. Owing to the Mach 1.5 primary jet, the inner modes associated with the inner shear layer display supersonic phase speeds. Conversely, the outer modes have subsonic phase speeds, as the secondary jet is subsonic. At this frequency ($St = 0.3$), the outer modes are more unstable than the inner ones. It must be noted, however, that such comparisons are confounded by normalization issues – the outer modes'

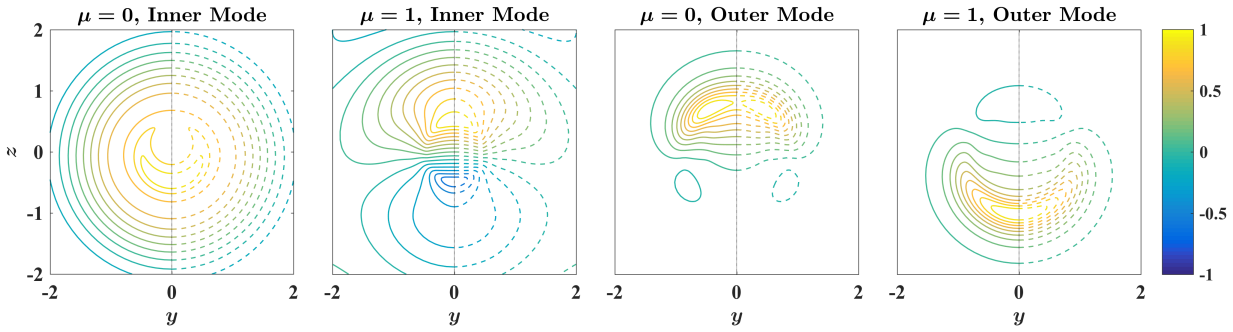

Figure 4: Offset jet: real parts of the normalized pressure eigenfunctions corresponding to the modes depicted in fig. 3. Shooting method results are as solid contours in the left halves, whereas those from the direct matrix approach are as dashed contours in the right halves.

Inner Modes

$\mu = 0$							$\mu = 1$						
Direct matrix			Shooting				Direct matrix			Shooting			
S	c_p	$-\alpha_i$	S	$\breve{N}$	c_p	$-\alpha_i$	S	c_p	$-\alpha_i$	S	$\breve{N}$	c_p	$-\alpha_i$
6	1.3338	0.2643	6	4	1.3338	0.2643	6	1.2602	0.2916	6	4	1.2602	0.2916
8	1.3338	0.2643	8	6	1.3338	0.2643	8	1.2602	0.2916	8	6	1.2602	0.2916

Outer Modes

$\mu = 0$							$\mu = 1$						
Direct matrix			Shooting				Direct matrix			Shooting			
S	c_p	$-\alpha_i$	S	$\breve{N}$	c_p	$-\alpha_i$	S	c_p	$-\alpha_i$	S	$\breve{N}$	c_p	$-\alpha_i$
15	0.6179	0.2772	15	9	0.6179	0.2770	11	0.5990	0.4040	11	8	0.5990	0.4040
16	0.6179	0.2770	15	10	0.6179	0.2770	12	0.5990	0.4040	12	9	0.5990	0.4040

Table 1: Offset jet: convergence of eigenvalues in four modes calculated by the two methods. Parameter set cases used in eigenfunction investigations are highlighted.

results should rightly be normalized with the outer jet parameters for that exercise.

Figure 4 shows the real part of the pressure eigenfunctions corresponding to the four modes described above. The 'far' shooting solution for an eigenfunction is adjusted with a complex scalar to match its 'centre' solution counterpart at the intermediate radial grid point. Subsequently, the eigenfunction is normalized to have a maximum of unity over the $y-z$ domain; moreover, the phase of the complex function is set to vanish at the point of maximum. The normalization is consistently applied to the direct matrix method results also.

The departure from axisymmetry due to the offset is apparent, although the mirror symmetry is preserved. The mean flow depicted in fig. 1a should be referred for orientation of the axes maintained consistent here. The inner modes can be seen to peak around the inner shear layer ($r \approx 0.5$) and the outer modes are maximum around the outer shear layer ($r \approx 0.85$). Recall that r is normalized by the primary nozzle exit diameter, and the diameter ratio of the two nozzles is 1.7.

The rationale of the $\mu = 0$ and $\mu = 1$ nomenclature is apparent for the inner modes, but is confounded for the outer modes. Thus, this nomenclature should be considered as merely a way of labelling eigensolutions here. More meaning can be ascribed to these labels when the modes are tracked starting from the concentric jet case (where the azimuthal Fourier modes are decoupled) by varying the offset, as described by Singh et al. [9].

Table 1 establishes the convergence of the eigensolution calculations with the direct matrix method

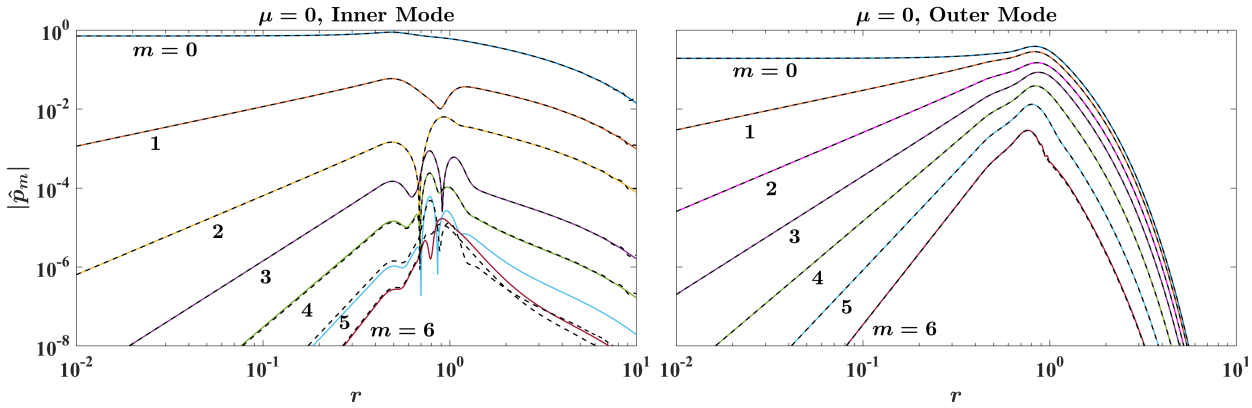

Figure 5: Offset jet: normalized pressure eigenfunctions of the outer and inner modes for $\mu = 0$. Coloured solid lines and black dashed lines are from the shooting and direct matrix methods, respectively.

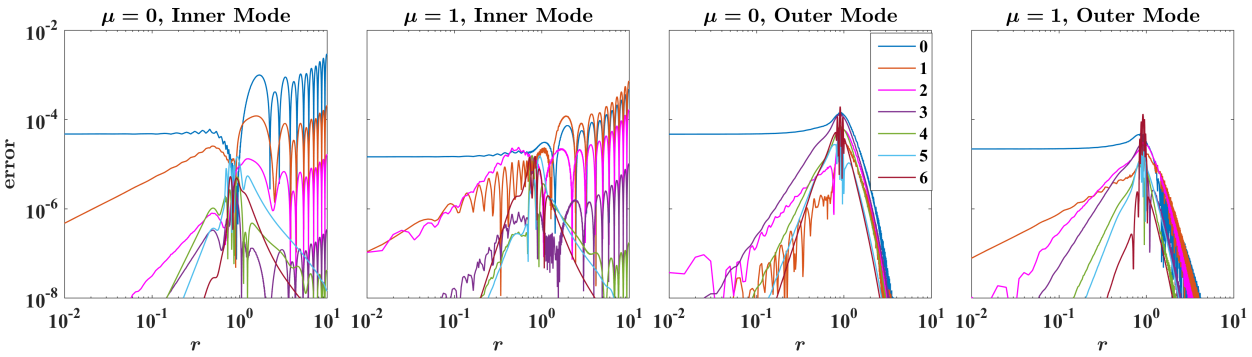

Figure 6: Offset jet: absolute value of differences between the direct and shooting method results for the normalized pressure eigenfunctions of the inner and outer modes of both $\mu = 0$ and 1 cases. The legend shows the mode numbers m of the various coupled azimuthal Fourier modes depicted.

with respect to the eigenfunctions' azimuthal modal complexity S. In the shooting method, the important parameters for convergence are S, as well as the azimuthal modal complexity $\breve{N}$ of the mean flow functions $\hat{\overline{f}}$, $\hat{\overline{g}}$ and $\hat{\overline{h}}$. Recall that the azimuthal complexity of the mean flow field itself is held at $N = 3$ for all these calculations for the purpose of comparison, as it forms the common input to both the methods. The results in table 1 thus demonstrates that the shooting method replicates the eigenvalues from the direct matrix approach up to the fourth place of decimal, as depicted in fig. 3 also.

Table 1 also demonstrates the different azimuthal complexities of the inner and outer modes. The inner shear layer is almost axisymmetric, the centreline being set to the centre of the primary jet. The asymmetry due to the offset between the two streams mainly manifests in the outer shear layer, thereby necessitating more azimuthal modes for the representation of the corresponding eigensolution.

The validation of the eigenfunctions was demonstrated in fig. 4; in fact, the contours from the two approaches were so similar in this representation that they were not overlaid to reduce visual clutter. A further demonstration of the similarity of the results from the two methods appears in fig. 5, where we resort to the azimuthal Fourier domain and plot the coupled modes as in fig. 2. The first few azimuthal modes of the pressure eigenfunction are shown for $\mu = 0$ in both the inner and outer modes. The direct matrix method results are overlaid on those from the shooting approach, and the differences are indeed very small. The inner mode decays slowly toward the far field, and shows somewhat greater discrepancy than the outer mode; this is explained below.

The minor differences are further highlighted in fig. 6, which also extends the presentation to the $\mu = 1$ modes. The normalized eigenfunctions of the outer mode calculated by the two approaches differ by less than 1 part in 10,000. The inner mode cases show greater discrepancies, as expected from fig. 5.

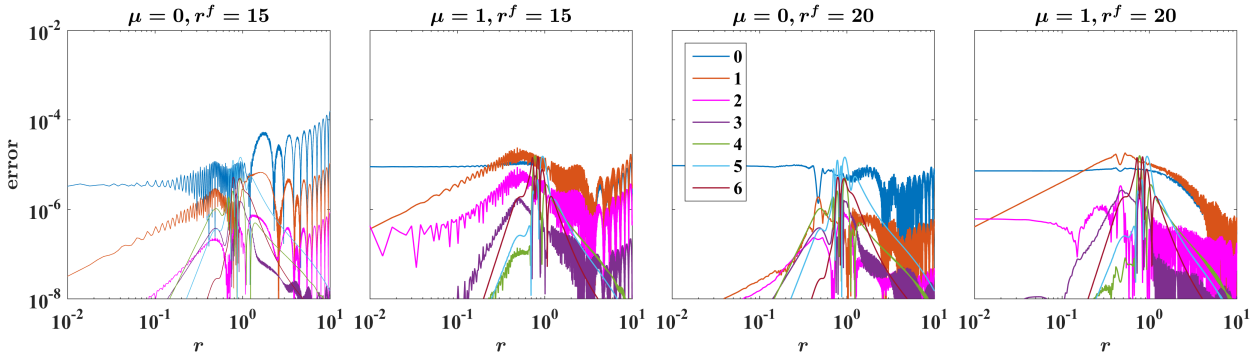

Figure 7: Offset jet: reduction in the discrepancies between the shooting and direct matrix eigenfunctions for the $\mu = 0$ and 1 inner modes by furthering of the far-field boundary r^f in the latter approach.

$M = 0$							$M = 1$						
Direct matrix			Shooting				Direct matrix			Shooting			
S	c_p	$-\alpha_i$	S	$\breve{N}$	c_p	$-\alpha_i$	S	c_p	$-\alpha_i$	S	$\breve{N}$	c_p	$-\alpha_i$
1	0.7453	0.2236	1	1	0.7452	0.2221	1	0.6638	0.2181	1	1	0.6651	0.2145
2	0.7446	0.2215	2	1	0.7448	0.2231	2	0.6608	0.2136	2	1	0.6618	0.2193
3	0.7445	0.2215	2	2	0.7445	0.2216	3	0.6606	0.2145	2	2	0.6607	0.2141
4	0.7445	0.2215					4	0.6606	0.2146				

Table 2: Chevron jet: convergence of eigenvalues in two modes calculated by the two methods. Parameter set cases used in eigenfunction investigations are highlighted.

To determine the cause of the discrepancy in the inner mode eigenfunction results, the direct matrix calculation of these modes is repeated with larger values of r^f, the 'far-field' radius where we apply the characteristic boundary condition of Thompson [11]. The results heretofore have been obtained with $r^f = 10$ for both the shooting and direct matrix methods. Without redoing the shooting calculations, we evaluate their discrepancy against the direct matrix results recalculated with $r^f = 15$ and 20. Figure 7 demonstrates that this reduces the error drastically; the eigenvalues were found to remain unchanged. Apparently, the inner modes have sufficient amplitude at $r = 10$ (see fig. 5), so that the characteristic boundary condition in the direct matrix approach is inappropriate at this point. It is interesting to note that the shooting method fares much better in this regard as it implements an analytical boundary condition that only requires the mean flow to be uniform at the boundary.

Finally, we note the parameters of the calculations that were not discussed above. For the shooting method, the 'centre' solution calculation was started from $r^c = 0.01$, whereas the 'far' solution was initiated from $r^f = 10$. The Runge-Kutta solver `ode45` of MATLAB® takes steps of variable size; however, on an average about 5000 points were automatically evaluated in this interval. For the direct method, the number of radial grid points N_r was 2000 in all the calculations, even when r^f was increased for the cases presented in fig. 7. Changing this did not affect the results materially.

B. Validation with single-stream chevron jet

The second validation case is the jet exiting from the 6-chevron nozzle sliced at $x = 3$ (see fig. 1a). We solve for the $M = 0$ and 1 eigensolutions for $St = 0.3$. The azimuthal modal complexity of the mean flow was $N = 1$ at this axial station. That is, only the $m = 0$ and 6 azimuthal modes of the mean axial velocity are relevant (see fig. 1b).

The results from the convergence study are presented in table 2. The direct matrix method is seen to be converged with $S = 3$. The eigenvalues thus calculated are matched closely by those from the shooting approach with $S = 2$ and $\breve{N} = 2$.

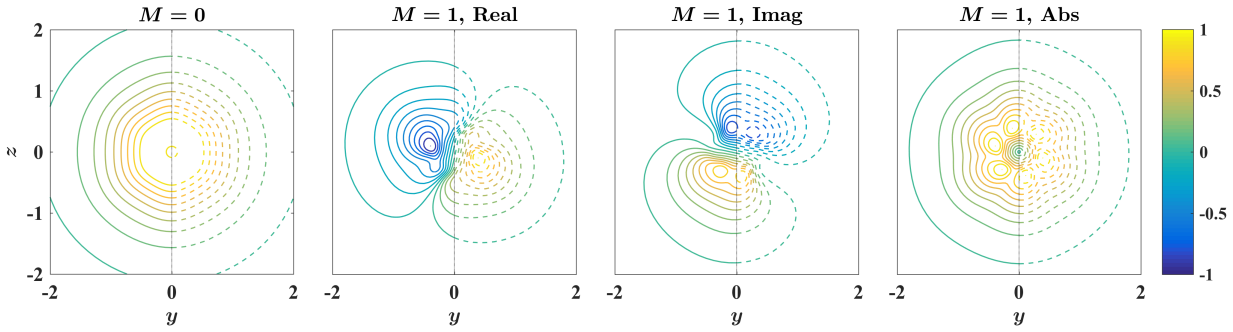

Figure 8: Chevron jet: leftmost pane shows real parts of the normalized $M = 0$ pressure eigenfunctions. Remaining panes show real, imaginary and absolute values of the $M = 1$ eigenfunctions. Shooting method results are as solid contours in the left halves, whereas those from the direct matrix approach are as dashed contours in the right halves.

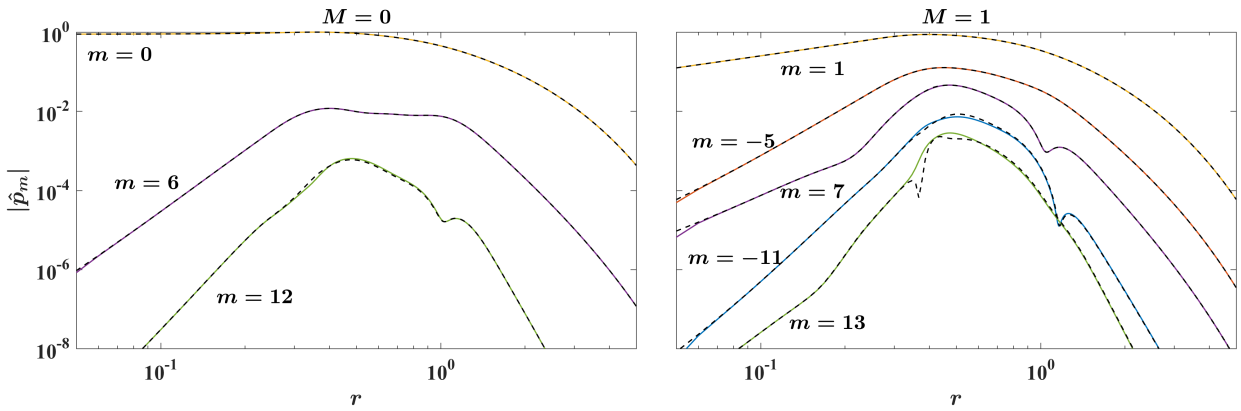

Figure 9: Chevron jet: normalized pressure eigenfunctions of the $M = 0$ and 1 modes. Coloured solid lines and black dashed lines are from the shooting and direct matrix methods, respectively.

Figure 8 presents the eigenfunctions corresponding to these two modes. The real part of the $M = 0$ pressure eigenfunction displays a 6-fold rotational symmetry and mirror symmetry; the latter is similar to the offset jet results. Neither of these symmetries are apparent in the real (or imaginary) part of the $M = 1$ eigenfunction. However, the absolute value of the same displays the 6-fold rotational symmetry. Note that the absolute value of the $M = -1$ eigenfunction is mirror symmetric with its $M = 1$ counterpart. These are known properties of the eigenfunctions of chevron jets, and discussed extensively by Sinha et al. [7].

Figure 8 also demonstrates the match of the eigenfunctions between the two approaches. This is further clarified in figs. 9 and 10. The very low discrepancies serve to validate the shooting approach.

We faced some numerical issues in the shooting calculations for the chevron jet, as discussed below. With 6 chevrons, every 6th azimuthal mode is coupled in the eigensolution. Figure 9 shows that the values of these successive coupled pressure eigenfunctions drop by several orders of magnitude at the centre and far boundaries. It will be recalled that the shooting approach attempts to determine these very ratios (viz. $\hat{p}^c_6/\hat{p}^c_0\,|_{r=r^c}$, $\hat{p}^c_{12}/\hat{p}^c_0\,|_{r=r^c}$, $\hat{p}^f_6\Big/\hat{p}^f_0\Big|_{r=r^f}$, $\hat{p}^f_{12}\Big/\hat{p}^f_0\Big|_{r=r^f}$, etc. for the $M = 0$ calculation), in an iterative manner so as to satisfy the matching criteria at the intermediate radial point. It is the extremely small values of these ratios that make the numerical computation ill-conditioned when more azimuthal modes of the solution are coupled (i.e., higher S values are considered). Specifically, the Jacobian of the cost function becomes poorly conditioned.

The problem was mitigated somewhat by limiting the radial domain – we started the 'centre' shooting from $r^c = 0.05$ and the 'far' shooting from $r^f = 5$. Even with this, we could not obtain converged results for $S > 2$. Further curtailing of the radial domain is not warranted as the mean axial velocity becomes

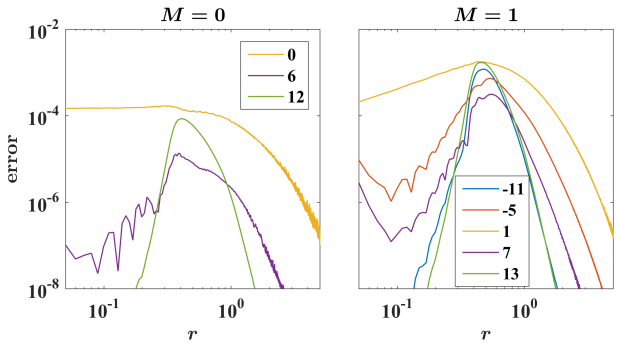

Figure 10: Chevron jet: absolute value of differences between the direct and shooting method results for the normalized pressure eigenfunctions of the $M = 0$ and 1 modes. The legend shows the mode numbers m of the various coupled azimuthal Fourier modes depicted.

non-uniform otherwise, invalidating the boundary conditions formulated. A future workaround will be to start higher-order modes from successively closer to the lip-line, so that the initial values of the various pressure modes are never less than the precision afforded by double-precision arithmetic.

To conclude the discussion, we note that in the direct method, r^f was set to 10, and $N_r = 600$ radial grid points was found to be sufficient for convergence.

VI. Conclusions

This paper describes a shooting approach to solve the bi-global inviscid parallel-flow stability problem for non-axisymmetric jets. The shooting method is especially useful in tracking eigensolutions in parametric sweeps. The solution obtained with one set of parameters may be conveniently used as the initial condition for solving with another parameter set that is not too different from the first, thereby hastening convergence.

To the authors' knowledge, Gudmundsson [6] gives the only other report of the formulation of the shooting method for the bi-global problem. We implemented three important improvements to the algorithm – viz. (a) a two-way integration approach for increased numerical stability, (b) analytical evaluation of the Jacobian of the cost function, and (c) explicit implementation of mirror symmetry to halve the problem size wherever possible. Apart from detailing the formulation, we provide extensive evidence of the validity of our approach. Indeed, results from two jet cases are compared against the direct matrix approach to the same problem, and excellent agreement is demonstrated in all the tests.

In this paper, we have not discussed the advantages of shooting method over the direct matrix approach with regards to computational efficiency, due to differences in implementation. The direct matrix method has been implemented in Fortran, and it is parallelized. Calculations are run on tens of processors, and results are obtained within a few minutes on a cluster of Intel Xeon multi-core processors, depending on the complexity of the calculation and the number of eigenvalues desired. On the other hand, the shooting method is implemented in serial mode in MATLAB®, and calculations take a few minutes on a MacBook Air laptop. Thus, while precise comparison would require commensurate codes and architecture, one can still draw conclusions on the substantial efficiency of the shooting method vis-à-vis the direct matrix approach.

APPENDIX

A. Eigenfunction symmetry in mirror-symmetric base flow

To deduce the azimuthal Fourier symmetry of the eigenfunctions of a mirror-symmetric base flow, we replace m (assumed to be positive) by $-m$ and j by $-j$ in eqn. (7) to obtain

$$\frac{1}{r}\frac{\partial}{\partial r}\left(r\frac{\partial \hat{p}_{-m}}{\partial r}\right) - \frac{m^2}{r^2}\hat{p}_{-m} - \sum_{j=-\infty}^{\infty}\left\{\hat{\bar{f}}_{-Lj}\frac{\partial}{\partial r} + \frac{\iota(-m+Lj)}{r^2}\hat{\bar{g}}_{-Lj} + \hat{\bar{h}}_{-Lj}\right\}\hat{p}_{-m+Lj} = 0, \qquad \forall m > 0.$$

Applying the symmetry properties of $\hat{\bar{f}}$, $\hat{\bar{g}}$ and $\hat{\bar{h}}$ introduced in eqn. (9), we obtain

$$\frac{1}{r}\frac{\partial}{\partial r}\left(r\frac{\partial \hat{p}_{-m}}{\partial r}\right) - \frac{m^2}{r^2}\hat{p}_{-m} - \sum_{j=-\infty}^{\infty}\left\{\hat{\bar{f}}_{Lj}\frac{\partial}{\partial r} + \frac{\iota(m-Lj)}{r^2}\hat{\bar{g}}_{Lj} + \hat{\bar{h}}_{Lj}\right\}\hat{p}_{-(m-Lj)} = 0, \qquad \forall m > 0.$$

Comparison with eqn. (7) reveals that $\hat{p}_{-m} = \hat{p}_m$.

B. Analytically Evaluating the Jacobian

We describe the analytical evaluation of the Jacobian $\mathbb{J}$ of the cost function vector $\boldsymbol{\Gamma}$ with respect to the parameter vector $\boldsymbol{V}$. Equation (14) shows that $\boldsymbol{\Gamma}$ has two kinds of entries, viz, Λ_m and Λ'_m, for various azimuthal modes m. It will be recalled that $m \in \{M + Lj\}_{j=-S}^{S}$ in general, whereas $m \in \{Lj\}_{j=0}^{S}$ for the $M = 0$ azimuthal order of eigenfunction in mirror symmetric base flows. On the other hand, eqn. (12) shows that $\boldsymbol{V}$ consists of α, U_n^c and U_n^f for various azimuthal modes n. In general $n \in \{M + Lj\}_{j=-S}^{S}$ with $n \neq M$, but $n \in \{Lj\}_{j=1}^{S}$ in the special case of the $M = 0$ solution in mirror symmetric base flows. The evaluation of the Jacobian thus requires the following derivatives at $r = r_i$:

$$\frac{\partial \Lambda_m}{\partial \alpha} = \frac{\partial \hat{p}_m^c}{\partial \alpha} - \frac{\hat{p}_m^f}{\hat{p}_M^f}\frac{\partial \hat{p}_M^c}{\partial \alpha} - \frac{\hat{p}_M^c}{\hat{p}_M^f}\left(\frac{\partial \hat{p}_m^f}{\partial \alpha} - \frac{\hat{p}_m^f}{\hat{p}_M^f}\frac{\partial \hat{p}_M^f}{\partial \alpha}\right),$$

$$\frac{\partial \Lambda'_m}{\partial \alpha} = \frac{\partial^2 \hat{p}_m^c}{\partial \alpha \partial r} - \frac{1}{\hat{p}_M^f}\frac{\partial \hat{p}_M^c}{\partial \alpha}\frac{\partial \hat{p}_m^f}{\partial r} - \frac{\hat{p}_M^c}{\hat{p}_M^f}\left(\frac{\partial^2 \hat{p}_m^f}{\partial \alpha \partial r} - \frac{1}{\hat{p}_M^f}\frac{\partial \hat{p}_M^f}{\partial \alpha}\frac{\partial \hat{p}_m^f}{\partial r}\right),$$

$$\frac{\partial \Lambda_m}{\partial U_n^c} = \frac{\partial \hat{p}_m^c}{\partial U_n^c} - \frac{\hat{p}_m^f}{\hat{p}_M^f}\frac{\partial \hat{p}_M^c}{\partial U_n^c}, \qquad \frac{\partial \Lambda_m}{\partial U_n^f} = \frac{\hat{p}_M^c}{\hat{p}_M^f}\left(\frac{\hat{p}_m^f}{\hat{p}_M^f}\frac{\partial \hat{p}_M^f}{\partial U_n^f} - \frac{\partial \hat{p}_m^f}{\partial U_n^f}\right),$$

$$\frac{\partial \Lambda'_m}{\partial U_n^c} = \frac{\partial^2 \hat{p}_m^c}{\partial U_n^c \partial r} - \frac{1}{\hat{p}_M^f}\frac{\partial \hat{p}_M^c}{\partial U_n^c}\frac{\partial \hat{p}_m^f}{\partial r}, \qquad \frac{\partial \Lambda'_m}{\partial U_n^f} = \frac{\hat{p}_M^c}{\hat{p}_M^f}\left(\frac{1}{\hat{p}_M^f}\frac{\partial \hat{p}_m^f}{\partial r}\frac{\partial \hat{p}_M^f}{\partial U_n^f} - \frac{\partial^2 \hat{p}_m^f}{\partial U_n^f \partial r}\right).$$

The above expressions further suggest that we require the following set of quantities at the intermediate radial point r_i in order to evaluate the Jacobian:

$$\left\{\hat{p}_m^\zeta, \frac{\partial \hat{p}_m^\zeta}{\partial r}, \frac{\partial \hat{p}_m^\zeta}{\partial \alpha}, \frac{\partial^2 \hat{p}_m^\zeta}{\partial \alpha \partial r}, \frac{\partial \hat{p}_m^\zeta}{\partial U_n^\zeta}, \frac{\partial^2 \hat{p}_m^\zeta}{\partial U_n^\zeta \partial r}\right\}, \qquad \zeta \in \{c, f\}. \tag{16}$$

In the above, Einstein summing convention does not apply to repeated ζ indices. The first two quantities are found by default in the integration of the eigenfunction itself. To determine the four other quantities, we need to integrate them from the two boundaries also. Thus, the set of quantities in eqn. (16) actually constitute the augmented vector to be integrated. The necessary initial conditions at the boundaries for these additional terms are found as the corresponding derivatives of the boundary conditions in eqns. (11) and (13):

$$\left.\frac{\partial \hat{p}_m^\zeta}{\partial \alpha}\right|_{r=r^\zeta} = U_m^\zeta r^\zeta \frac{\partial \lambda^\zeta}{\partial \alpha} B'_m\left(\lambda^\zeta r^\zeta\right), \qquad \left.\frac{\partial \hat{p}_m^\zeta}{\partial U_n^\zeta}\right|_{r=r^\zeta} = B_m\left(\lambda^\zeta r^\zeta\right)\delta_{m,n},$$

$$\left.\frac{\partial^2 \hat{p}_m^\zeta}{\partial \alpha \partial r}\right|_{r=r^\zeta} = U_m^\zeta \frac{\partial \lambda^\zeta}{\partial \alpha}\left\{B'_m\left(\lambda^\zeta r^\zeta\right) + r^\zeta \lambda^\zeta B''_m\left(\lambda^\zeta r^\zeta\right)\right\}, \qquad \left.\frac{\partial^2 \hat{p}_m^\zeta}{\partial U_n^\zeta \partial r}\right|_{r=r^\zeta} = \lambda^\zeta B'_m\left(\lambda^\zeta r^\zeta\right)\delta_{m,n}.$$

As before, the pair (ζ, B) takes values in (c, I) or (f, K).

We differentiate eqn. (7) with respect to the relevant entries of $\boldsymbol{V}$ (viz. α and U_n^ζ) to obtain the second-order ODEs governing the last four quantities in the augmented integration vector of eqn. (16):

$$\frac{1}{r}\frac{\partial}{\partial r}\left(r\frac{\partial^2 \hat{p}_m^\zeta}{\partial r \partial \alpha}\right) - \frac{m^2}{r^2}\frac{\partial \hat{p}_m^\zeta}{\partial \alpha} - \sum_{j=-\infty}^{\infty}\left\{\hat{\bar{f}}_{Lj}\frac{\partial}{\partial r} + \frac{\iota(m-Lj)}{r^2}\hat{\bar{g}}_{Lj} + \hat{\bar{h}}_{Lj}\right\}\frac{\partial \hat{p}_{m-Lj}^\zeta}{\partial \alpha}$$
$$- \sum_{j=-\infty}^{\infty}\left\{\frac{\partial \hat{\bar{f}}_{Lj}}{\partial \alpha}\frac{\partial}{\partial r} + \frac{\iota(m-Lj)}{r^2}\frac{\partial \hat{\bar{g}}_{Lj}}{\partial \alpha} + \frac{\partial \hat{\bar{h}}_{Lj}}{\partial \alpha}\right\}\hat{p}_{m-Lj}^\zeta = 0, \tag{17}$$

$$\frac{1}{r}\frac{\partial}{\partial r}\left(r\frac{\partial^2 \hat{p}_m^\zeta}{\partial r \partial U_n^\zeta}\right) - \frac{m^2}{r^2}\frac{\partial \hat{p}_m^\zeta}{\partial U_n^\zeta} - \sum_{j=-\infty}^{\infty}\left\{\hat{\bar{f}}_{Lj}\frac{\partial}{\partial r} + \frac{\iota(m-Lj)}{r^2}\hat{\bar{g}}_{Lj} + \hat{\bar{h}}_{Lj}\right\}\frac{\partial \hat{p}_{m-Lj}^\zeta}{\partial U_n^\zeta} = 0. \tag{18}$$

References

[1] J. E. Bridges and C. A. Brown. Parametric testing of chevrons on single flow hot jets. In *10th AIAA/CEAS Aeroacoustics Conference, AIAA Paper 2824*, 2004.

[2] V. H. Arakeri, A. Krothapalli, V. Siddavaram, M. B. Alkislar, and L. M. Lourenco. On the use of microjets to suppress turbulence in a Mach 0.9 axisymmetric jet. *Journal of Fluid Mechanics*, 490:75–98, 2003.

[3] E. Murakami and D. Papamoschou. Mean flow development in dual-stream compressible jets. *AIAA Journal*, 40(6): 1131–1137, 2002.

[4] P. Jordan and T. Colonius. Wave packets and turbulent jet noise. *Annual Review of Fluid Mechanics*, 45:173–195, 2013.

[5] K. Gudmundsson and T. Colonius. Spatial stability analysis of chevron jet profiles. In *13th AIAA/CEAS Aeroacoustics Conference, AIAA Paper 3599*, 2007.

[6] K. Gudmundsson. *Instability wave models of turbulent jets from round and serrated nozzles*. PhD thesis, California Institute of Technology, 2010.

[7] A. Sinha, K. Gudmundsson, H. Xia, and T. Colonius. Parabolized stability analysis of jets from serrated nozzles. *Journal of Fluid Mechanics*, 789:36–63, 2016.

[8] N. Sohoni and A. Sinha. Modelling noise sources in offset two-stream jets using linear stability theory. In *2018 AIAA/CEAS Aeroacoustics Conference, AIAA Paper 3941*, 2018.

[9] N. Singh, N. Sohoni, and A. Sinha. Modelling noise sources in offset two-stream jets using linear stability theory – further developments. In *25th AIAA/CEAS Aeroacoustics Conference*, 2019, accepted.

[10] K. Mohseni and T. Colonius. Numerical treatment of polar coordinate singularities. *Journal of Computational Physics*, 157:787–795, 2000.

[11] K. W. Thompson. Time dependent boundary conditions for hyperbolic systems. *Journal of Computational Physics*, 68: 1–24, 1987.

[12] R. B. Lehoucq, D. C. Sorensen, and C. Yang. *ARPACK users' guide: solution of large-scale eigenvalue problems with implicitly restarted Arnoldi methods*. SIAM, 1998.

[13] P. J. Schmid and D. S. Henningson. *Stability and transition in shear flows*. Springer, 2001.

[14] M. Gloor, D. Obrist, and L. Kleiser. Linear stability and acoustic characteristics of compressible, viscous, subsonic coaxial jet flow. *Physics of Fluids*, 25:084102, 2013.